Advances in Water Resources 142 (2020) 103631

Contents lists available at ScienceDirect

Advances in Water Resources

journal homepage: www.elsevier.com/locate/advwatres

Impact of time-dependent wettability alteration on the dynamics of capillary pressure

Abay Molla Kassa[a,b,*], Sarah Eileen Gasda[a], Kundan Kumar[b], Florin Adrian Radu[b]

[a] NORCE Norwegian Research Center, Bergen, Norway
[b] Department of Mathematics, University of Bergen, Norway

ARTICLE INFO

Keywords:
Wettability alteration
Dynamic capillary pressure
Dynamic wettability
Bundle-of-tubes simulation
Upscaling

ABSTRACT

Wettability is a pore-scale property that has an important impact on capillarity, residual trapping, and hysteresis in porous media systems. In many applications, the wettability of the rock surface is assumed to be constant in time and uniform in space. However, many fluids are capable of altering the wettability of rock surfaces permanently and dynamically in time. Experiments have shown wettability alteration (WA) can significantly decrease capillarity in CO_2 storage applications. For these systems, the standard capillary-pressure model that assumes static wettability is insufficient to describe the physics. In this paper, we develop a new dynamic capillary-pressure model that takes into account changes in wettability at the pore-level by adding a dynamic term to the standard capillary pressure function. We assume a pore-scale WA mechanism that follows a sorption-based model that is dependent on exposure time to a WA agent. This model is coupled with a bundle-of-tubes (BoT) model to simulate time-dependent WA induced capillary pressure data. The resulting capillary pressure curves are then used to quantify the dynamic component of the capillary pressure function. This study shows the importance of time-dependent wettability for determining capillary pressure over timescales of months to years. The impact of wettability has implications for experimental methodology as well as macroscale simulation of wettability-altering fluids.

1. Introduction

Wettability plays an important role in many industrial applications, in particular subsurface porous media applications such as enhanced oil recovery (EOR) and CO_2 storage (Blunt, 2001; Bonn et al., 2009; Iglauer et al., 2014, 2016; Yu et al., 2008). The wetting property of a given multiphase system in porous media is defined by the distribution of contact angles. The contact angle (CA) is controlled by surface chemistry and associated forces acting at the molecular scale along the fluid-fluid-solid interface (Bonn et al., 2009). In porous media applications, microscale wettability determines the strength of pore-scale capillary forces and the movement of fluid interfaces between individual pores. At the core-scale, wettability impacts upscaled quantities and constitutive functions such as residual saturation, relative permeability, and capillary pressure, which in turn affect field-scale multiphase flow behavior.

The standard assumption is that wettability is a static property of the multiphase system. However, the composition of many fluids is capable of provoking the surfaces within pores to undergo wettability alteration (WA) via a change in CA. CA change can alter capillary forces at the pore scale, and thus affect residual saturations of the system (Ahmed and Patzek, 2003; Blunt, 1997). This effect has been exploited extensively in the petroleum industry, where optimal wetting conditions in the reservoir are obtained through a variety of means that includes chemical treatment, foams, surfactants, and low-salinity water flooding (see for example Morrow et al., 1986; Buckley et al., 1988; Jadhunandan and Morrow, 1995; Haagh et al., 2017; Singh and Mohanty, 2016).

Wettability is also recognized as a critical factor in geological CO_2 sequestration which exerts an important role on caprock performance (Kim et al., 2012; Tokunaga and Wan, 2013). The sealing potential of the caprock is highly dependent on CO_2 being a strongly non-wetting fluid, and WA may lead to conditions that allow for buoyant CO_2 to leak (Chiquet et al., 2007a; Chalbaud et al., 2009). Besides, WA can affect residual saturation and subsequently impact the trapping efficiency of injected CO_2 (Iglauer et al., 2014). Therefore, reliable quantification of wettability is needed for safe and effective CO_2 storage.

Despite the fact that WA is known to impact core-scale capillarity and relative permeability behavior, few detailed measurements are available to characterize the alteration of the constitutive function themselves. Plug and Bruining (2007) have reported brine-CO_2 (gas, liquid) drainage-imbibition experiment and showed capillary instability for a

* Corresponding author at: NORCE Norwegian Research Center, Bergen, Norway.
E-mail address: abka@norceresearch.no (A.M. Kassa).

https://doi.org/10.1016/j.advwatres.2020.103631
Received 10 July 2019; Received in revised form 6 May 2020; Accepted 15 May 2020
Available online 20 May 2020

supercritical CO_2-brine system, meaning that the capillary pressure measurements change steadily over time. The imbibition curve also exhibited a significant deviation from the expected curve that was not explained by classical scaling arguments. The authors proposed WA as an explanation but did not explicitly measure any changes in CA. Additionally, recent experiments measured capillary pressure curves for a silicate sample using a fluid pairing of supercritical CO_2 and brine (Wang and Tokunaga, 2015). Repeated drainage-imbibition cycles were performed for 6 months, and a clear reduction in capillary pressure was recorded for each subsequent drainage cycle. The authors also attributed these deviations from the expected capillary curve to a change in wettability of the rock sample over time due to CO_2 exposure, similar to aging. This hypothesis was confirmed through observations of a wetting angle increase from 0° to 75° after 6-months of exposure. It is also reported similar $P_c - S$ instability and deviation in dolomite/carbonate (Wang et al., 2016), and quartz (Tokunaga et al., 2013; Wang et al., 2016) sands for $scCO_2$ -brine system. More literature on WA and $P_c - S$ measurements can be found in (Tokunaga and Wan, 2013).

The above experiments reveal that capillary pressure curves are not static for rocks that undergo WA, despite the fact they were performed following the standard multi-step procedure, i.e. where "equilibrium" is obtained after each incremental step in pressure. Therefore, the standard capillary pressure models cannot be readily applied without additional dynamics to capture the long-term impact of WA. Capillary pressure dynamics due to WA are distinct from non-equilibrium flow dynamics (e.g. Hassanizadeh et al., 2002; Dahle et al., 2005; Barenblatt et al., 2003) or from CA hysteresis generated by receding and advancing angles (e.g. Krumpfer and McCarthy, 2010; Eral et al., 2013). WA alteration is a chemistry-induced pore-scale phenomenon that alters the capillary pressure function separately from the flow conditions or other instabilities. That is, contact angle has the potential to change even when the system is at rest. On the other hand, NE models are formulated to address dynamics in only for systems that are flowing, and therefore a new approach is needed to account for permanent and continual alteration of capillary pressure functions for both flowing and non-flowing systems. We note that capillary driven flow may initiate if the CA change is large.

The standard approach to WA is to assume a change in surface chemistry that occurs instantaneously, which results in an immediate shift in saturation functions (Delshad et al., 2009; Lashgari et al., 2016; Yu et al., 2008; Andersen et al., 2015; Adibhatia et al., 2005). This implementation entails a heuristic approach that interpolates between the two end wetting states as a linear function of chemical agent concentration. Lashgari et al. (2016) have derived an instantaneous WA model from Gibbs energy and adsorption isotherms. The proposed WA model is coupled with $P_c - S$ relation through residual saturation. These models neglect the impact of WA over longer timescales (months to years). They also do not capture pore-scale heterogeneity in wetting properties. In the available literature, only one study (Al-Mutairi et al., 2012) has included the effect of exposure time on WA and constitutive relations for core scale simulation. But this numerical study does not sufficiently incorporate or upscale pore-scale processes to core-scale constitutive laws.

To our knowledge, a rigorous mathematical upscaling of long-term dynamics in $P_c - S$ functions introduced by exposure to a WA agent has not been previously performed. The focus of this paper is to propose a new dynamic capillary pressure model by upscaling the WA dynamics from the pore- to the core-scale. Section 2 describes our approach. We start with direct simulations of $P_c - S$ curves from a pore-scale model represented by a cylindrical bundle-of-tubes. WA is introduced at the pore scale using a mechanistic model for CA change as a function of exposure time to a reactive agent. This model is developed based on the insights from laboratory experiments, giving the flexibility to incorporate other data as appropriate. We emphasize the CA model is only meant as a basis on which to demonstrate the upscaling approach. In Section 3, we present the resulting curves generated by the pore-scale model using two different pore-scale models for CA change. These curves are then used to correlate the dynamic term in the upscaled $P_c - S$ function. Finally, we analyze the link between pore-scale parameters and upscaled correlations.

2. Approach

The extended $P_c - S$ relationship introduces a dynamic component that captures the changing wettability as measured by the deviation of the dynamic capillary pressure from the equilibrium (static) capillary pressure. This relationship can be described as follows:

$$P_c(\cdot) - P_c^{\mathrm{st,in}} := f^{\mathrm{dyn}}(\cdot), \tag{1}$$

where $P_c^{\mathrm{st,in}}$ represents the capillary pressure for the system given a static initial wetting state, and f^{dyn} represents the deviation from the static state. The initial static curve can be described by the Brooks-Corey model,

$$P_c^{\mathrm{st,in}} = c_w \left(\frac{S_w - S_{wc}}{1 - S_{wc}} \right)^{-a_w}, \tag{2}$$

where c_w is the entry pressure, $1/a_w$ is the pore-size distribution index, whereas S_{wc} is the residual water saturation.

The objective of this study is to characterize and quantify the dynamic term f^{dyn}, the key term of interest in the $P_c - S$ model, for a system that undergoes WA. We propose an interpolation model to handle the WA dynamics in $P_c - S$ relation. To obtain an interpolation model, the dynamic component in Eq. (1) can be scaled by the difference between two static curves, each representing the initial and final wetting-state capillary pressure curves, to give a non-dimensional quantity ω we call the *dynamic coefficient*, which is defined as follows

$$\omega \left(P_c^{\mathrm{st,f}} - P_c^{\mathrm{st,in}} \right) = f^{\mathrm{dyn}}, \tag{3}$$

where $P_c^{\mathrm{st,f}}$ is the final wetting state capillary pressure. In the previous studies (e.g. see Delshad et al., 2009; Lashgari et al., 2016; Yu et al., 2008; Andersen et al., 2015; Adibhatia et al., 2005), the coefficient ω is assumed only chemistry dependent. Here, ω in Eq. (3) is assumed to be a function of not only the chemistry but also the exposure time to the WA agent.

The expression in Eq. (3) can be substituted into Eq. (1) to obtain a dynamic interpolation model

$$P_c = (1 - \omega) P_c^{\mathrm{st,in}} + \omega P_c^{\mathrm{st,f}}. \tag{4}$$

We note that in the model presented above, we have defined the "total" capillary pressure P_c as simply the measured difference in phase pressures at any point in time. In a reservoir simulation, this would be capillary pressure in a given grid cell, whereas in a laboratory experiment designed to measure $P_c - S$ data, it corresponds to the pressure drop across the sample at equilibrium. For quasi-static displacement in a bundle of capillary tubes, P_c is the difference between boundary condition pressures, i.e., $P_c = P_l^{res} - P_r^{res}$, (see Fig. 1).

The exact nature of ω and its functional dependencies can only be determined from a full characterization of $P_c - S$ curves under different conditions. These curves can be derived from laboratory experiments, but this approach is costly and time-consuming. Alternatively, one may take a more theoretical approach by simulating $P_c - S$ curves using a pore-scale model that includes the impact of WA.

For a system that undergoes WA, a significant change in CA could lead to the wetting phase becoming non-wetting and vice versa. For clarity, we will continue to use *w* subscript for the phase that was originally wetting and *nw* for the phase that is originally non-wetting regardless of the actual state of wettability in the system.

2.1. Pore-scale model

There are various choices of pore-scale models available. The easiest to implement and analyze is the bundle-of-tubes (BoT) model which is a collection of capillary tubes with a distribution of radii. Herein, we

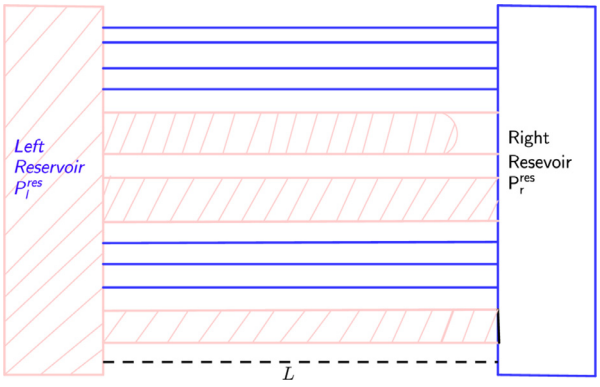

Fig. 1. Fluid displacement in a non-interactive bundle-of-tubes (BoT). Here, the left reservoir contains non-wetting fluid that displaces the wetting fluid to the right and vice versa.

describe the model and the approach for the implementation of time-dependent WA.

The BoT model is a popular approach due to the simplicity of implementation and the ability to study the balance of energy and forces directly at the scale of interfaces (Bartley and Ruth, 1999; Dahle et al., 2005; Helland and Skjæveland, 2006). The average behavior of a BoT model can then be used to construct better constitutive functions at the macroscale (Dahle et al., 2005; Helland and Skjæveland, 2006; 2007). There are known limitations to this pore-scale approach, i.e. lack of residual saturation and tortuosity. We emphasize that this study is a first step at studying the impact of long-term WA from pore- to core-scale, and as such these secondary aspects are beyond the scope of this work.

In this paper, we consider cylindrical BoT having length, L, and is shown in Fig. 1. These tubes are designed to connect wetting (right) and non-wetting (left) reservoirs with pressures labeled as $P_{\mathrm{r}}^{\mathrm{res.}}$ and $P_l^{\mathrm{res.}}$ respectively. Let the reservoir pressures difference be defined as

$$\Delta P = P_l^{res} - P_r^{res}. \tag{5}$$

Initially, the tubes in the bundle are filled with a wetting phase. To displace the wetting phase fluid in the m^{th} tube, the pressure drop has to exceed the local entry pressure, $P_{c,m}$, defined as (Dahle et al., 2005)

$$\Delta P > P_{c,m}(R_m, \theta_m), \tag{6}$$

where $P_{c,m}(R_m, \theta_m)$ is given by the Young's equation

$$P_{c,m}(R_m, \theta_m) = \frac{2\sigma\cos(\theta_m)}{R_m}, \ m = 1, 2, \cdots, N, \tag{7}$$

where R_m and θ_m are the tube radius and CA, respectively, for the m^{th} tube, N stands for number of tubes, σ is fluid-fluid interfacial tension.

As long as condition (6) is satisfied, the fluid movement across the length of tube m can be approximated by the Lucas-Washburn flow model (Washburn, 1921),

$$q_m = \frac{R_m^2(\Delta P - P_{c,m}(R_m, \theta_m))}{8(\mu_{\mathrm{nw}} x_m^{int} + \mu_{\mathrm{w}}(L - x_m^{int}))}, \tag{8}$$

where, μ_{nw} and μ_{w} are non-wetting and wetting fluid viscosities, respectively, the superscript *int* stands for fluid-fluid interface, and $q_m = dx_m^{int}/dt$ is the interface velocity. The interface is assumed to be trapped when it reached at the outlet of the tube, thus $q_m = 0$. A positive rate of change in x_m^{int} is associated with an increase in non-wetting saturation for tube m. From Eq. (8), one can then determine the required time to reach a specified interface position.

2.2. Pore-scale time-dependent WA model

In this paper, we consider a WA mechanism at the pore-scale that evolves smoothly from an initial to final wetting state through exposure time. The initial and final wetting states can be arbitrarily chosen, i.e. from wetting to non-wetting or vice versa.

The WA agent is defined as either the non-wetting fluid itself or some reactive component therein. We consider an alteration process within any given pore, or tube, that continues until the ultimate wetting state is reached locally in the pore. The alteration is permanent, but can also be halted at some intermediate wettability state if the WA agent is displaced from the pore. If the agent is reintroduced to the pore at some later point, alteration continues until the final state is reached.

To this end, we introduce a general functional form of pore-scale WA mechanism by CA change,

$$\theta_m(\cdot) := \theta_{m,\mathrm{in}} + \varphi(\cdot)\Delta\Theta, \tag{9}$$

where $\Delta\Theta = \theta_{m,\mathrm{f}} - \theta_{m,\mathrm{in}}$, $\theta_{m,\mathrm{f}}$ and $\theta_{m,\mathrm{in}}$ are the ultimate and initial contact angles respectively. In Eq. (9), θ_m decreases and increases based on the choice of the initial and final wetting conditions. The term $\varphi(\cdot) \in [0, 1]$ (when $\varphi(\cdot) = 1$ the CA attains its ultimate value and CA is fixed at the initial state when $\varphi(\cdot) = 0$) in Eq. (9) is responsible for governing the WA dynamics.

WA involves complex physical and chemical processes whose description is beyond the scope of this work. However, we provide a brief summary of the role of adsorption/desorption processes in CA change (Blut, 2017; Du et al., 2019). Such a hypothesis has been supported by experiment measurements. For instance, CO_2-water core-flooding experiments show adsorption-type relations between CA and pressure (Dickson et al., 2006; Jung and Wan, 2012; Iglauer et al., 2012), and also with exposure time (Jafari and Jung, 2016; Saraji et al., 2013). Similar CA evolutions as a function of surfactant concentration and exposure time are reported in Davis et al. (2003) and (Morton et al., 2005) for an oil droplet on a metal surface immersed in ionic surfactant solutions. In Morton et al. (2004), a Langmuir adsorption model is proposed to predict the experiment observations in (Davis et al., 2003). Given the insights above, we consider a CA model that evolves according to the rate of adsorption of the WA agent on the surface of the pores. Following McKee (1991), van Erp et al. (2014), the dynamic parameter φ in Eq. (9) can be stated as,

$$\frac{d\varphi}{dt} = J^+ - J^-, \tag{10}$$

where J^+ and J^- represent rates of adsorption and desorption of a WA agent respectively at the solid surface. In McKee (1991), J^+ is taken to be proportional to the WA agent and the surface unoccupied by the adsorbed WA agent, i.e.,

$$J^+ = k_1\chi_m\left(1 - \varphi/\overline{\varphi}\right), \tag{11}$$

where k_1 is a rate constant, $\overline{\varphi}$ represents the maximum surface saturated concentration, and χ_m is a measure of the local exposure time of tube m. The desorption rate can be related with the current surface concentration and is defined as,

$$J^- = k_2\varphi \tag{12}$$

where k_2 is a rate constant for desorption rate. Combining Eqs. (10)–(12) would give us,

$$\frac{d\varphi}{dt} = k_1\chi_m\left(1 - \varphi/\overline{\varphi}\right) - k_2\varphi. \tag{13}$$

Assuming $\overline{\varphi} = 1$ and following McKee (1991), one can apply a perturbation analysis to Eq. (13) to obtain a first-order approximation for φ in terms of χ_m,

$$\varphi \approx \frac{\chi_m}{C + \chi_m}, \tag{14}$$

where $C = \frac{k_2}{k_1}$ is a parameter that controls the speed and extent of alteration. χ_m is defined as the time-integration of exposure to a WA agent, here taken to be the local non-wetting saturation of tube m,

$$\chi_m := \frac{1}{T}\int_0^t \frac{x_m^{int}}{L} d\tau, \tag{15}$$

where T is a pre-specified characteristic time. In this paper, the characteristic time is set as the time for one complete drainage displacement under static initial wetting conditions, which can be pre-computed according to Eq. (8).

As an aside, detailed laboratory work would be needed to further enrich the pore-scale CA model by fitting C to experimental data. This exercise is beyond the scope of this paper, and we consider the underlying CA change in Eq. (14) a reasonable basis for which to perform the upscaling aspect of our study.

Herein, we consider two models for exposure time at the local scale. For first we take the case where CA modification based on Eq. (14) is strictly dependent on local exposure time χ_m and leads to CA variation from tube to tube, hereafter referred to as the *non-uniform WA* mechanism. We note that wettability gradients within individual tubes are not considered in this model, and thus there is no variation in CA along the tube. This is due to the flow model in Eq. (8), where the CA only affects the entry pressure of the tube.

The second is referred to as *uniform WA*, which is based on the assumption that the WA agent dissolves into the wetting phase from the non-wetting fluid and affects all tubes simultaneously. In this case, all tubes have the same properties that are governed by the bulk exposure time across the entire bundle (i.e. REV). We can define $\overline{\chi}$

$$\overline{\chi} := \frac{1}{T}\int_0^t S_{nw}\, d\tau. \tag{16}$$

as the bulk or average, exposure time as a function of average saturation. The uniform model is implemented into Eq. (14) by taking $\chi_m = \overline{\chi}$.

In summary, we introduce two types of WA mechanisms, uniform and non-uniform, that serve as end members of possible WA mechanisms at the pore-scale. On the one end, non-uniform WA restricts alteration to only drained pores and excludes any interaction of the WA agent between pores. This leads to significant heterogeneity in CA from one pore to another. At the other end, the uniform case assumes the WA agent can alter all pores simultaneously. In reality, WA will lie somewhere in between, but we have chosen simpler end members to aid in further analysis of simulated data in the next section.

2.3. Simulation approach

The uniform and non-uniform approaches are coupled into the BoT model following Algorithm 1 for a single drainage-imbibition cycle. The objective is to perform simulated experiments that mimic laboratory-derived capillary pressure curves, i.e. the pressure is adjusted incrementally up or down after each step depending on if the bundle is under drainage or imbibition, respectively. Contact angles are updated continuously throughout the flow processes in a step-wise manner once the displacement is completed for each pressure increment. That is, contact angles that have been altered according to the uniform or non-uniform mechanism, are updated before the next pressure increment. This is a reasonable approximation given that it is only entry pressures in individual tubes that are affected by CA change.

We control the pressure drop ΔP in the way that the WA process is completed within a few numbers of drainage-imbibition cycles. In the first drainage-imbibition cycles, the ΔP increment is such that tubes drain/imbibe one at a time with a pressure drop close to the next tube entry pressure. In the last drainage-imbibition cycle, every ΔP increment is reduced by two and three orders of magnitude for the non-uniform and uniform case, respectively. Consequently, the flow slows down by the same magnitude irrespective of whether the tube drains or imbibes. At the completion of the numerical experiment, we obtain a set of $P_c - S$ "data points" that can be plotted in the usual way.

Once the capillary pressure curves are generated for both the uniform and non-uniform approaches, the resulting curves are used to quantify the dynamic coefficient in the interpolation function in Eq. (4). The goal is to develop a correlation model that involves only a single parameter, and this parameter should have a clear relation with changes in the pore-scale WA model parameter C.

Algorithm 1 A single drainage-imbibition cycle. Fluid and rock properties are given according to Table 2

```
Drainage displacement
set the maximum capillary pressure P_c^max
while ΔP < P_c^max do
    increase the non-wetting pressure, P_l^res
    calculate the pressure drop ΔP = P_l^res − P_r^res
    if ΔP > 2σ cos(θ_m)/R_m then
        drain the respective tubes
        calculate the elapse of time to drain tubes from Equation (8)
        calculate and store averaged quantities S_nw and χ̄
        if non-uniform WA then
            calculate χ_m for invaded pores from Equation (15)
            calculate θ_m from Equation (9) and (15)
        else if uniform WA then
            update each θ_m in bundle identically from Equation (9)
            and (16)
        end if
    end if
end while
Imbibition displacement
define the minimum entry pressure P_c^min
while ΔP > P_c^min do
    decrease the non-wetting pressure, P_l^res
    calculate the pressure drop ΔP = P_l^res − P_r^res
    if ΔP > σ cos(θ_m)/R_m then
        imbibe the respective tubes
        calculate the elapsed of time to imbibe tubes from
        Equation (8)
        calculate and store averaged quantities S_nw and χ̄
        if non-uniform WA then
            calculate χ_m from Equation (15)
            update θ_m from Equation (9) and (15)
        else if uniform WA then
            update each θ_m identically from Equation (9) and (16)
        end if
    end if
end while
```

3. Results

In this section, we present the simulated capillary pressure and associated results for each WA case. We formulate a correlation model, which is then fit to the simulated data. Finally, we investigate the sensitivity of the correlated model to the pore-scale WA parameter.

3.1. Bundle of tubes model set-up

The pore scale is described by a BoT model (see Section 2.1). Each tube in the BoT is assigned a different radius R, with the radii drawn from a truncated two-parameter Weibull distribution (Helland and Skjæveland, 2006)

$$f(R) = \frac{\left[\frac{R-R_{\min}}{R_{\text{av}}}\right]^{\eta-1}\frac{\eta}{R_{\text{av}}}\exp\left(-\left[\frac{R-R_{\min}}{R_{\text{av}}}\right]^{\eta}\right)}{1-\exp\left(-\left[\frac{R_{\max}-R_{\min}}{R_{\text{av}}}\right]^{\eta}\right)} \tag{17}$$

where $R_{\max}$, $R_{\min}$, and R_{av} are the pore radii of the largest, smallest, and average pore sizes, respectively, and η is a dimensionless parameter. The average is obtained by the mean of $R_{\max}$ and $R_{\min}$. The rock parameters and fluid properties are listed in Table 1.

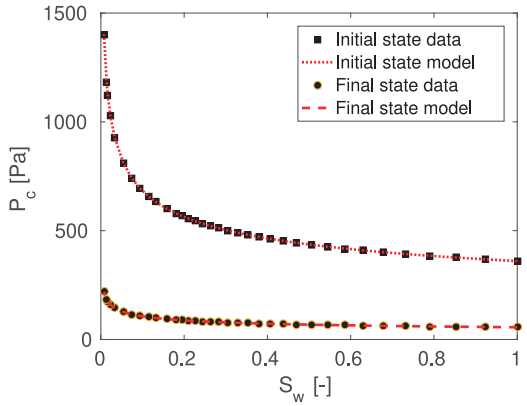

Fig. 2. Simulated $P_c - S$ data for the initial and final wetting states compared to a Brooks-Corey model with calibrated parameters given in Table 2.

3.2. Static capillary pressure for end wetting states

A starting point for the dynamic capillary-pressure models presented in Section 2 (Eqs. (1) and (4)) is characterizing the capillary pressure curves for the end wetting states. Given the same tube geometry and fluid pairing described above, the capillary pressure–saturation data are simulated under static conditions for both the initial and final wetting states.

Only a single drainage experiment is needed in the static case to fully characterize the capillary pressure curve. This is due to the lack of residual trapping in a BoT model. We emphasize that hysteresis is not possible for a BoT if the contact angles in the tubes (and other parameters) are held constant.

The simulated static curves are then correlated with the Brooks-Corey model (2). The resulting correlations can be found in Fig. 2, while fitted parameters for the Brooks-Corey model can be found in Table 2. Note that the Brooks-Corey model is undefined at zero irreducible wetting phase saturation. Thus, we left a few pores undrained to allow for comparison between the Brooks-Corey model and the simulated $P_c - S$ data.

Fig. 2 compares the Brooks-Corey formula (2) and the capillary pressure curves associated with static contact angles (initial and final wetting states).

The Brooks-Corey correlation gives an excellent match to the simulated $P_c - S$ data under static conditions. We observe that the pore-size distribution index a_w for the initial and final wetting states are the same, which is expected since the same distribution of tube radii is used in both cases. On the other hand, the coefficient c_w decreases by a factor of 0.85 from the initial to the final wetting state corresponding to a decrease in a core-scale capillary entry pressure. The Leverett-J scaling theory (Xu et al., 2016) predicts that entry pressure scales by $\cos\theta$, which agrees nicely with the reduction in $\cos\theta$ by a factor of 0.83 for a CA change from 0 to 80 degrees.

We reiterate that for the static case where no WA occurs, the Brooks-Corey model describes *both* drainage and imbibition for the BoT.

Table 1
Parameters used to simulate quasi-static fluid displacement in BoT.

parameters	values	unit	parameters	values	unit
σ_{ow}	0.0072	N/m	no. radii	500	[-]
$R_{\min}$	6	μm	$R_{\max}$	40	μm
θ_f	80	degree	θ_{in}	0.0	degree
μ_{w}	0.0015	Pa.s	μ_{nw}	0.0015	Pa.s
R_{av}	23	μm	L	0.001	m
η	1.5	[-]			

Table 2
Estimated correlation parameter values for initial and final wetting state capillary pressure curves.

Initial wetting state			Final wetting state		
param.	value	unit	param.	value	unit
c_w	360	[Pa]	c_w	56	[Pa]
a_w	0.2778	[-]	a_w	0.2778	[-]
R^2	1	-	R^2	1	-

3.3. Simulated capillary pressure data

We present the simulated capillary pressure data (see Fig. 3), comparing the results of the uniform and non-uniform approaches described previously. The uniform data are generated with the pore-scale WA parameter $C = 0.005$, while for the non-uniform data $C = 5 \times 10^{-4}$. A total of two and four drainage-imbibition cycles carried out for the uniform and non-uniform cases, respectively.

For both cases, we observe a steady decrease in capillary pressure over time. In the end, a complete wettability change has evolved from the initial to final prescribed states, whose static curves are plotted in Fig. 3 for reference. Having reached the final wetting state, any additional drainage-imbibition cycle would follow along the static curve for the final wetting state. We remark that wettability-induced dynamics also introduces an apparent hysteresis in the $P_c - S$ data. This effect is unique to the cylindrical BoT model, which we recall cannot exhibit hysteresis under static wettability conditions. However, a real porous medium may exhibit capillary pressure hysteresis with static wettability.

There are notable differences between the two sets of curves. For the uniform case (Fig. 3a), there are distinct curves for each drainage and imbibition displacement. The capillary pressure begins to decrease immediately and in a continuous manner over time. This is because the CA (Fig. 4a) is changing for all tubes simultaneously based on the average exposure time over the entire bundle. The uniformity results in the CA in smaller tubes being altered significantly at an early time (at the same rate as the larger tubes), and thus the capillary pressure is decreased even at low average wetting saturation in the first drainage curve. The fast dynamics in CA change lead to a non-monotone capillary curve at an early time.

In comparison, the non-uniform case (Fig. 3b) has a delay in exhibiting the effects of WA. The initial drainage curve is identical to the initial wetting static curve and all subsequent drainage curves follow along the previous imbibition curve. This is a result of the restriction on CA change to only tubes that are drained. In other words, at the tube-level, there is no change in entry pressure from the initial state (or the state after a single drainage-imbibition cycle) until that tube is drained. In contrast to the uniform case, the capillary pressure at low S_w is drawn towards the initial state. This can be described by examining the CA per tube radius in time, shown in Fig. 4b. Larger tubes that drain first and imbibe last, resulting in longer local exposure time, and thus more extensive CA change, compared to the smaller tubes that drain last and imbibe first. Therefore, the initial wetting state persists in the smaller tubes.

We recall that both the uniform and non-uniform cases are selected as end members of possible WA mechanisms in real porous media. In real systems, WA in different sized pores may occur in a more complex manner.

We have observed above that capillary pressure curves in Fig. 3a and b are not a unique function of saturation, that is, they exhibit hysteresis for this simple BoT geometry. We note that the $P_c - S$ data points are color-coded according to time evolved at each data point. This motivates a transformation of the data into the time domain by plotting against $\overline{\chi}$, as shown in Fig. 5 for both cases. In doing so, we obtain a unique function with respect to exposure time for both the uniform and non-uniform cases. We note that the curves in Fig. 5 show that the capillary

pressure increases and decreases with each drainage-imbibition cycle. In addition, the transformation reveals the separate drainage curves for the non-uniform case that were hidden in Fig. 3b.

3.4. Dynamic capillary pressure model development

Following the approach discussed in Section 2, we applied Eq. (3) to calculate the dynamic coefficient ω for both the uniform and non-uniform cases. The resulting coefficient is plotted in Fig. 6 as a function of both S_w (top panels) and $\overline{\chi}$ (bottom panels) for both WA cases. We recall that ω is a coefficient that interpolates between the capillary pressure at the initial and final wetting states at any given saturation, where $\omega = 0$ gives the initial capillary pressure and $\omega = 1$ gives the final $P_c - S$ curve.

For the uniform case, ω is a non-unique function of wetting-phase saturation, see Fig. 6a, but with values that are continuously increasing as the dynamic capillary pressure moves towards the final wetting state. For the non-uniform case, the dynamic coefficient in Fig. 6b also exhibits non-uniqueness with respect to saturation. Reflecting the $P_c - S$ data, the capillary pressure persists at the initial state at low saturation. This means that the value of ω decreases with decreasing S_w along the drainage path and increases only along imbibition paths. The complex relation of ω in saturation space makes it challenging to propose a functional form for $\omega - S_w$ relation in both cases.

Figs. 6c and 6d show that ω exhibits different behavior as a function of average exposure time. For the uniform case, Fig. 6c, ω is smoothly increasing and uniquely related to $\overline{\chi}$, mimicking the functional form of the pore-scale model in Eq. (9). On the other hand, the coefficient ω in the non-uniform case, Fig. 6d, is not monotonically increasing in $\overline{\chi}$ but continues to rise and fall with time despite the transformation to the temporal domain.

The curves in Fig. 6 give us important insight into the form of ω best suited to each WA case. We take each case in turn:

3.4.1. Uniform case

The smoothly varying functionality of ω and $\overline{\chi}$ in Fig. 6c motivates an adsorption-type model:

$$\omega = \frac{\overline{\chi}}{\beta_1 + \overline{\chi}}, \tag{18}$$

where β_1 is a fitting parameter obtained from the best fit to the simulated data in Fig. 6c. For this particular case, the calibrated parameter is estimated to be $\beta_1 = 0.01$.

The form of the dynamic $P_c - S$ model for the uniform case is obtained by substituting Eq. (18) into Eq. (4) to give:

$$P_c = \frac{\overline{\chi}}{\beta_1 + \overline{\chi}}\left(P_c^{\mathrm{st,f}} - P_c^{\mathrm{st,in}}\right) + P_c^{\mathrm{st,in}}. \tag{19}$$

3.4.2. Non-uniform case

The non-trivial behavior of ω in Fig. 6d makes it challenging to propose a functional relation between the dynamic coefficient ω and $\overline{\chi}$ directly as we did for the uniform WA case. Instead, we observe that ω in Fig. 6b has a well-behaved curvature for each drainage-imbibition cycle along the saturation history. Further, the curvature of each cycle is increasing with increasing exposure time. Given these insights, we proposed a model for the dynamic coefficient that has the following form,

$$\omega(S_w, \overline{\chi}) = \frac{S_w}{\alpha(\overline{\chi}) + S_w}, \tag{20}$$

where α controls the curvature of the $\omega - S_w$ curve for each drainage-imbibition cycle. Since ω is increasing function of exposure time, α should decrease along the averaged variable $\overline{\chi}$.

The function form of ω in Eq. (20) is then matched with the $\omega - S_w$ data to analyze the dynamics of α along $\overline{\chi}$. The obtained $\alpha - \overline{\chi}$ relation is decreasing as hypothesized and in particular has the follwing form,

$$\alpha(\overline{\chi}) = \beta_2/\overline{\chi}, \tag{21}$$

where β_2 is non-dimensional fitting parameter. For this particular simulation the parameter β_2 is estimated to be 0.004 for the four of drainage-imbibition cycles.

The form of the dynamic $P_c - S$ model for the non-uniform case is then obtained by substituting Eqs. (20) and (21) into Eq. (4):

$$P_c = \frac{\overline{\chi} S_w}{\beta_2 + \overline{\chi} S_w}\left(P_c^{\mathrm{st,f}} - P_c^{\mathrm{st,in}}\right) + P_c^{\mathrm{st,in}}. \tag{22}$$

The calibrated dynamic capillary pressure models in Eqs. (19) and (22) are compared with the simulated capillary pressure data in Fig. 3, with the results presented in Fig. 7 for each WA case. We observe that the proposed dynamic models agree well with simulated dynamic capillary pressure curves. The correlation coefficient for this comparison is $R^2 = 0.9921$ and $R^2 = 0.98$, for the uniform and non-uniform case, respectively. Thus, we have obtained a single-parameter model in both the uniform and non-uniform WA cases that describe the evolution of dynamic capillarity over multiple drainage-imbibition cycles rather than using a model consisting of multiple parameters that change with each cycle (or hysteresis models).

3.5. Model sensitivity to pore-scale model parameter

We hypothesize that parameters β_1 in Eq. (19) and β_2 in Eq. (22) are dependent on the parameter C in Eq. (9) that controls the dynamics of wettability alteration at the pore-scale. We investigate this sensitivity by repeating the capillary pressure simulations for different values of the pore-scale parameter C and determine the correlated value of β_1 and β_2 in each case.

For the uniform WA case, Fig. 8a shows that the interpolation model parameter is linearly proportional to the pore-scale model parameter, with a proportionality constant of 2. Thus, the relationship $\beta_1 = 2C$ can be used to predict the upscaled parameter directly from knowledge of the pore-scale process. In contrast, the non-uniform case in Fig. 8b shows a power law model, where $\beta_2 = b_1 C^{b_2}$ is correlated with estimated parameters of $b_1 = 3.3 \times 10^6$ and $b_2 = 1.8$.

The general form of dynamic capillary pressure model can now be obtained for the uniform WA by incorporating the relationship for β_1 in Eq. (19) :

$$P_c = \frac{\overline{\chi}}{2C + \overline{\chi}}\left(P_c^{\mathrm{st,f}} - P_c^{\mathrm{st,in}}\right) + P_c^{\mathrm{st,in}}. \tag{23}$$

Similarly, we obtain a general non-uniform model by substituting β_2 in Eq. (22)

$$P_c = \frac{\overline{\chi} S_w}{b_1 C^{b_2} + \overline{\chi} S_w}\left(P_c^{\mathrm{st,f}} - P_c^{\mathrm{st,in}}\right) + P_c^{\mathrm{st,in}}. \tag{24}$$

In their final form, the dynamic capillary pressure models in Eqs. (23) and (23) are dependent on two variables, saturation and time, and a single wettability parameter, C. The latter must be determined by fitting Eq. (9) with parameter C to laboratory experiments for a given sample exposed to a WA agent.

3.6. Applicability to arbitrary saturation history

We note that the saturation history used to generate the $P_c - S$ curves for the two WA cases in Figs. 3a and 3c can be thought of in each case as a single arbitrary path within an infinite number of possible paths. If a different path had been chosen, such as a flow reversal at intermediate saturation or a prolonged exposure time at a given saturation, it would result in entirely different capillary pressure dynamics.

In order to test the dynamic models developed in Eqs. (19) and (22) for any arbitrary saturation history, we generate many different $P_c - S$ curves by taking numerous different paths in the saturation-time domain. The resulting simulated data forms a surface with respect to saturation and exposure time as shown in Fig. 9a and b

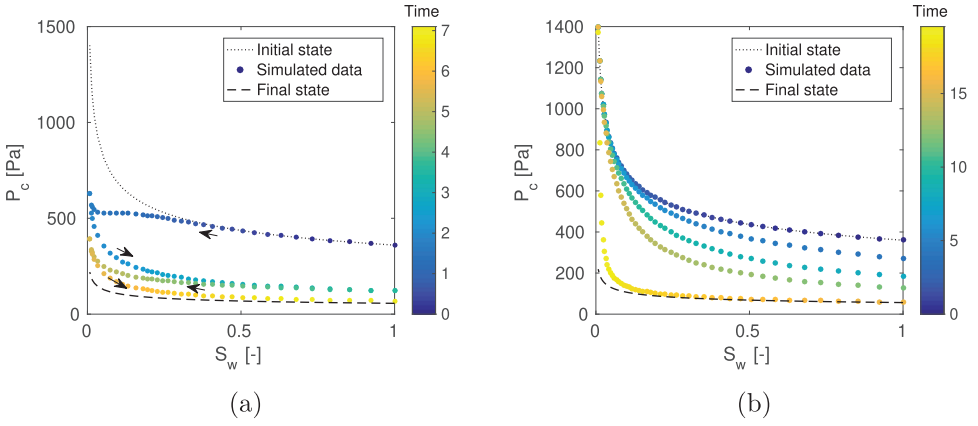

Fig. 3. Simulation results for WA-induced dynamics of capillary pressure as a function of wetting saturation given uniform (a) and non-uniform (b) WA at the pore-scale. The color of each data point indicates the time elapsed in months, with elapsed time equal to 7 months for the uniform case and 20 months for the non-uniform case. The data points are obtained following Algorithm 1. The static $P_c - S$ curves for the end wetting states, θ_{in} and θ_f, are plotted as a reference with dotted and dashed line, respectively.

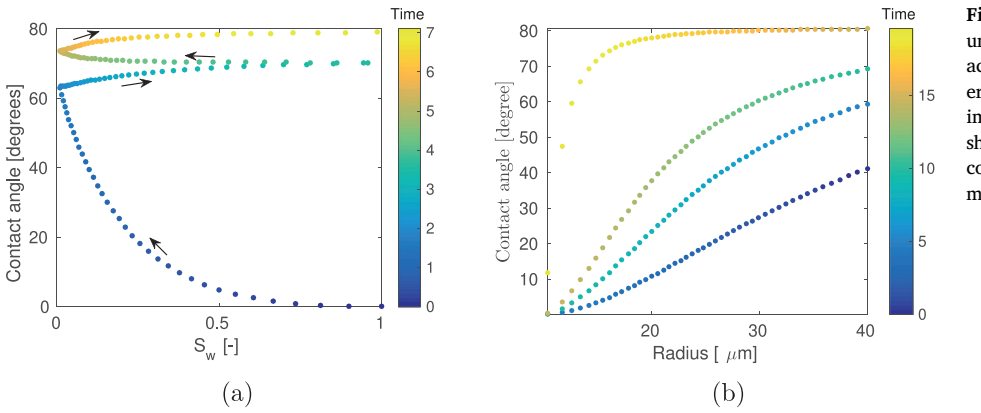

Fig. 4. CA, θ, for the uniform case (a) and non-uniform case (b). Uniform CA, which is identical across the bundle, is shown as a function of average saturation. The CA data show the drainage-imbibition fluid history paths. Non-uniform CA is shown as a function of tube radius and time. The color scale in both figures indicates time elapsed in months.

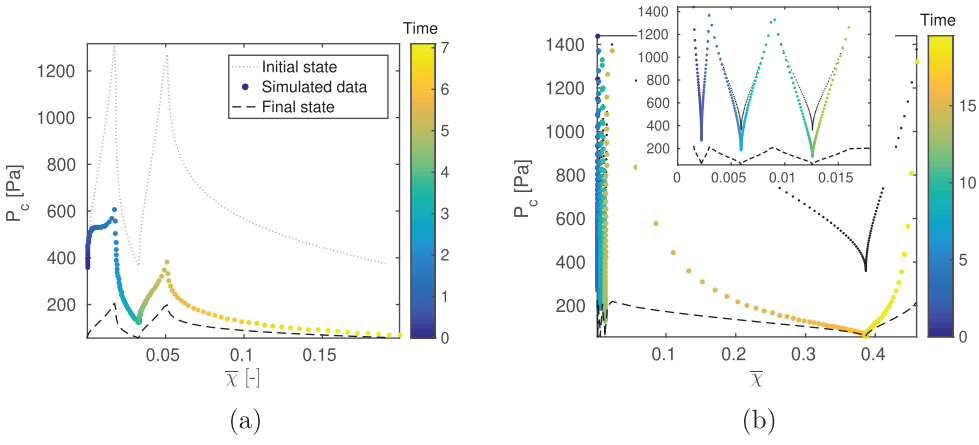

Fig. 5. Capillary pressure data plotted as a function of $\overline{\chi}$ for the uniform (a) and non-uniform (b) WA case. The color of each data point indicates the time elapsed in months. The inset plot in (b) is the resolution of the capillary pressure for the first three cycles.

We then apply the calibrated dynamic models to the same saturation-time paths used to generate the $P_c - S - \overline{\chi}$ surface. The difference between the calibrated model and the simulated data is shown in Fig. 9c and d for the uniform and non-uniform cases, respectively. A good comparison of the dynamic models to simulated data demonstrates that model calibration to a single saturation-time path is robust enough to be applied to any possible path.

3.7. Discussion

We investigated the potential of the interpolation-based model to predict the WA induced dynamics in capillary pressure–saturation relations. In the interest of completeness, we also explored other types of models to capture capillary pressure dynamics, including the mixed-wet model of Skjæveland et al. (2000). For brevity, we do not report the results of that separate study herein. We found that although other models could be calibrated with reasonable accuracy, they all involved more than one calibration parameter (up to four) that need to be adjusted in each drainage-imbibition cycle. Therefore, the single-parameter single-valued interpolation model presented in this study is the preferred model due to its reliability for replicating the simulated BoT data.

The proposed interpolation model is an upscaled model that allows for a change in capillary pressure as a function of upscaled variables, saturation, and exposure time, to a WA agent. We recall that exposure time is simply the integration of saturation history over time. The model consists of three main components – two capillary pressure functions at the initial and final wetting state and a dynamic interpolation coefficient that moves from one state to the other. The initial and final capillary

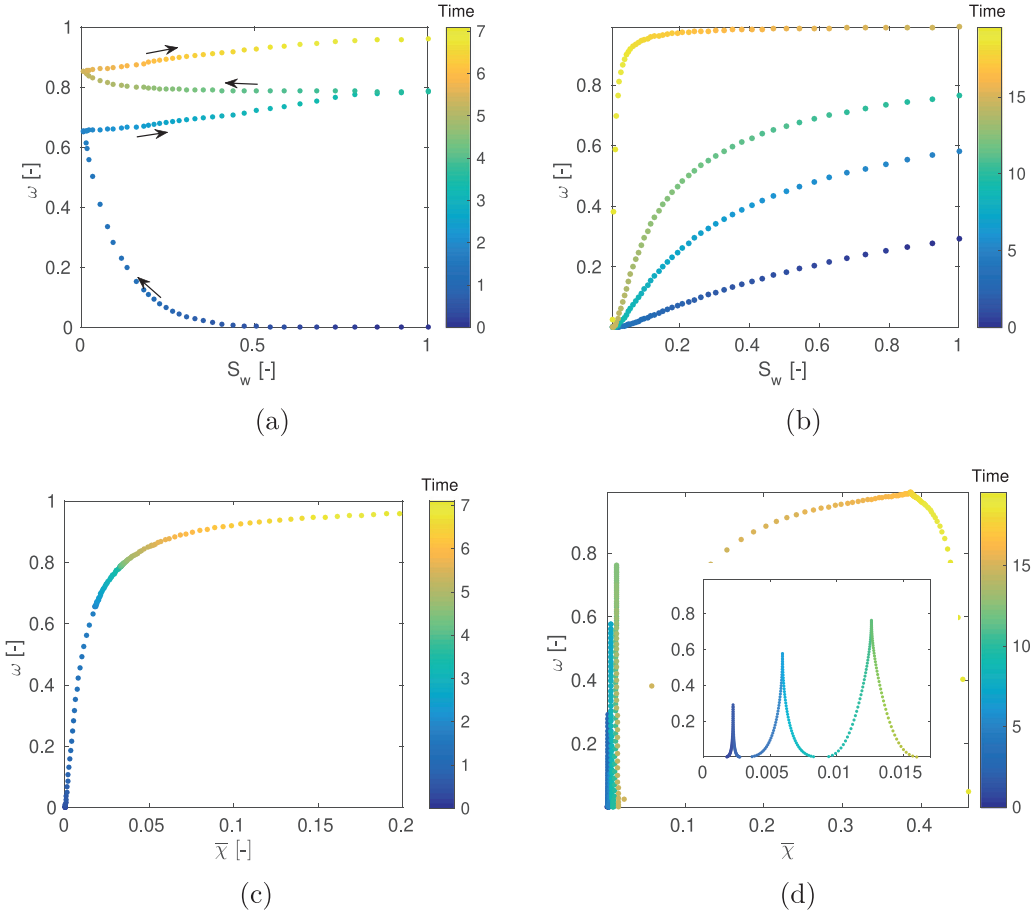

Fig. 6. Plot of the dynamic coefficient ω against wetting phase saturation (top) and $\overline{\chi}$ (bottom) for the uniform WA case (left panels) and non-uniform WA case (right panels). The data points are color-coded with exposure time in months. The inset plot in (d) is the resolution of the dynamic coefficient for the first three cycles.

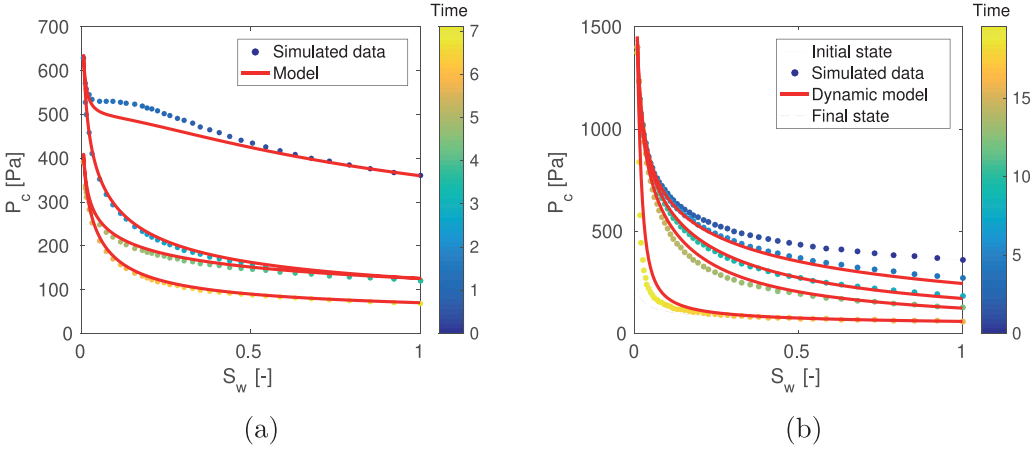

Fig. 7. Comparison of the dynamic models in Eqs. (19) and (22) with the simulated $P_c - S$ data in Fig. 3 for uniform (a) and non-uniform (b) WA cases. The data points are color-coded with exposure time in months.

pressure functions can be determined *a priori* from static experiments using inert fluids. In this study, the initial and final states are represented by classical Brooks-Corey functions. The dynamic coefficient is thus the only variable correlated to dynamic capillary pressure simulations. In this study, we have shown that the coefficient can be easily correlated to saturation and exposure time via a single parameter.

We have observed that the form of the dynamic term is dependent on the underlying mechanisms for WA. We employed two models, uniform and non-uniform, that represent two end members of real systems. One end member is identical CA throughout the REV, while the other results in severely heterogeneous CA from small to large pores. The differences in the two WA mechanisms changes the complexity of the resulting capillary dynamics. In the uniform case, the dynamic coefficient can be correlated to exposure time through a sorption-type model, which seems to be a natural result given the CA change at the pore scale is also based on a sorption model. This is an interesting observation that requires more analysis in future work. In the non-uniform case, the dynamic coefficient has no similar sorption form with increased exposure time, but

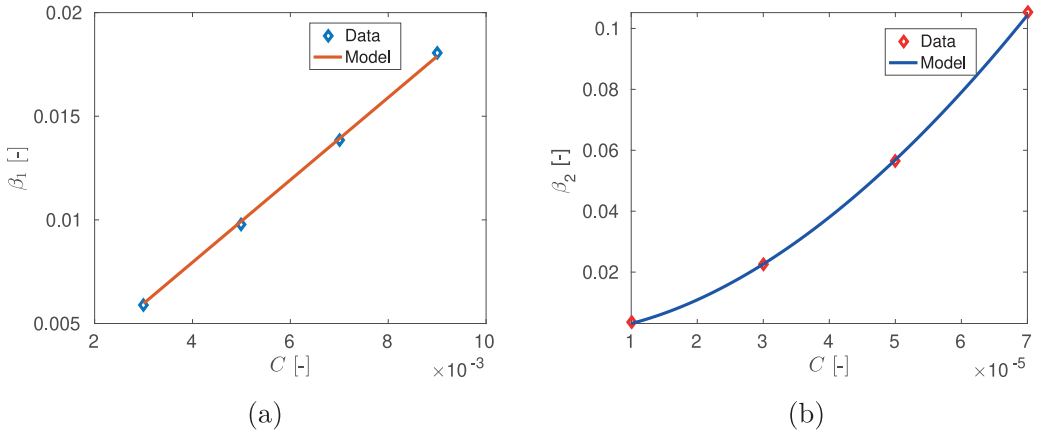

Fig. 8. The relation between pore-scale wettability parameter C and the correlation parameters β_1 and β_2 in Eqs. (19) and (22) for the uniform (a) and non-uniform (b) WA cases, respectively.

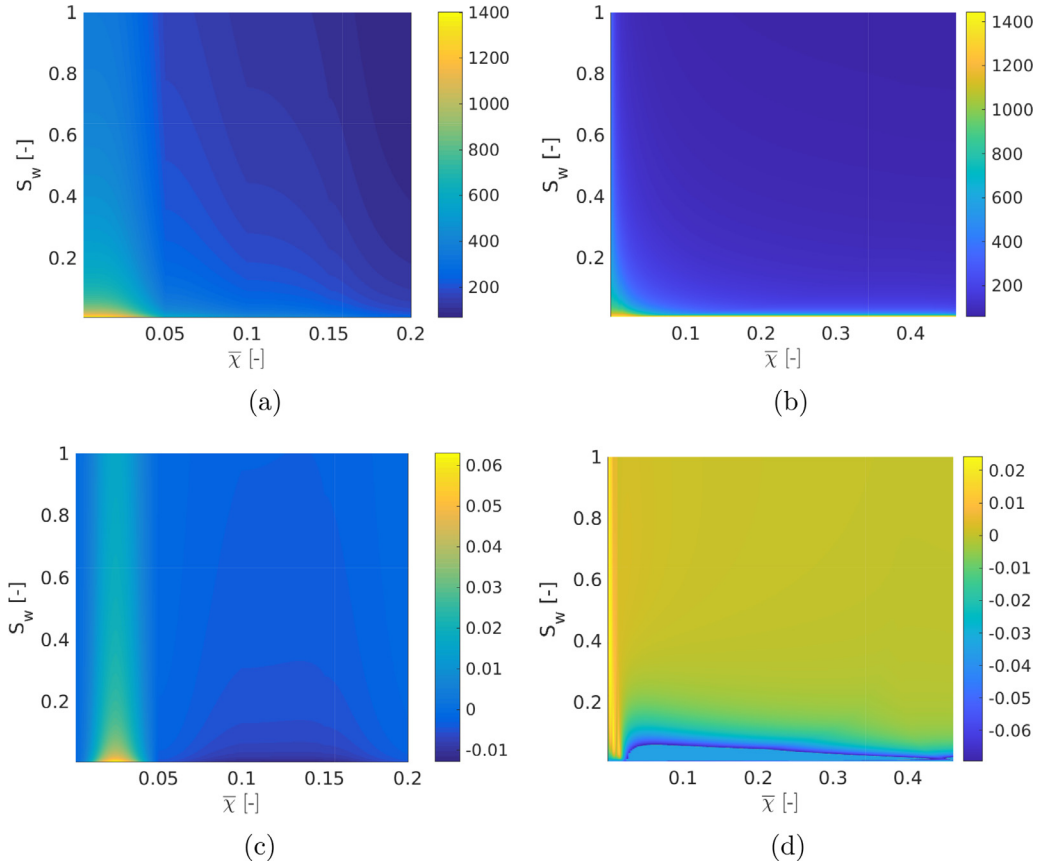

Fig. 9. *Top*: Simulated capillary pressure obtained by taking multiple paths in the $S_w \times \overline{\chi}$ domain, for the uniform (left) and non-uniform (right) cases. *Bottom*: The difference between the dynamic model (23) with the respective data, scaled by $P_c^{\max}$.

now with the product of saturation and exposure time as the dynamic variable. The additional complexity is needed to draw the capillary pressure curve back to the initial wetting at low saturation (a region of the $P_c - S$ curve dominated by smaller pores where the CA takes longer to change).

An important result of this study is quantifying the link between the pore- and core-scale. We showed that by varying the parameter that alters the speed and extent of CA change in each individual pore, we could predict the resulting impact on dynamic capillary pressure. In fact, in both the uniform and non-uniform cases, there is a very simple scaling from the pore-scale and macroscale parameters. In the uniform case, the two parameters are directly proportional, while in the non-uniform case, the macroscale parameter scales with the pore-scale parameter via a power law. The implication of this result is that by knowing the mechanism that controls CA at the pore-scale, which can be obtained by a relatively simple batch experiment, we can quantify *a priori* the macroscale dynamics without having to perform pore-scale simulations. This is an important generalization and valuable for making use of experimental data to inform macroscale constitutive functions.

We have quantified the ability of the interpolation model to capture underlying WA at the pore-scale for a simple BoT. This result is a natural development from previous studies that incorporate the interpo-

lation model directly into reservoir simulation of wettability alteration. In those studies, the model was matched directly to core-scale data in a heuristic manner. The contribution of this study is to quantify the pore-scale underpinnings to the interpolation model through a direct and systematic manner, thus providing additional evidence to the validity of this type of model for use in macroscale simulation.

Despite the satisfactory and relatively straightforward correlation of the interpolation model to simulated $P_c - S$ data, the exact quantification of the dynamics is ultimately restricted by the simplicity of the BoT model. We chose this simple approach in order to isolate the WA process from other complexities associated with real pore networks, and thus begin to assess the mechanisms linking the pore- and core-scales. Though beyond the scope of the current work, further study is needed to determine whether the fundamental nature of dynamic behavior we observe will hold when additional complexity is added. Further advancements can be made by adding complexity to the porous media (i.e. converging-diverging throat diameters or tortuosity) or to the pore-scale WA model. Theoretical work using pore-network models should also be combined with laboratory investigations to further calibrate the underlying WA mechanisms.

4. Conclusions

In this paper, we designed a framework to upscale the impact of time-dependent WA mechanisms at the pore scale on the dynamics in capillary pressure-saturation functions at the Darcy-scale. We found that an interpolation-based dynamic model can predict the change in capillary pressure due to underlying WA. The form of the dynamic interpolation coefficient is dependent on exposure time to a chemical agent, with a different mathematical form depending on the pore-scale WA mechanism. The correlated dynamic capillary pressure model shows an excellent match with simulated Pc-S data and reliably predicts capillary dynamics independent of the saturation-time path. More importantly, the model relies on a single interpolation parameter that has a clear and simple relationship with the pore-scale WA parameter.

CRediT authorship contribution statement

Abay Molla Kassa: Conceptualization, Data curation, Writing - original draft, Writing - review & editing. **Sarah Eileen Gasda:** Conceptualization, Data curation, Writing - original draft, Writing - review & editing. **Kundan Kumar:** Writing - review & editing. **Florin Adrian Radu:** Writing - review & editing.

Acknowledgement

Funding for this study was through the CHI project (n. 255510) granted through the CLIMIT program of the Research Council of Norway.

References

Adibhatia, B., Sun, X., Mohanty, K., 2005. Numerical studies of oil production from initially oil-wet fracture blocks by surfactant brine imbibition. In: SPE International Improved Oil Recovery Conference in Asia. SPE J. https://doi.org/10.2118/97687-MS.

Ahmed, A., Patzek, T.W., 2003. Impact of wettability alteration on two-phase flow characteristics of sandstones: a quasi-static description. Water Resour. Res. 39, 1–12. https://doi.org/10.1029/2002WR001366.

Al-Mutairi, S.M., Abu-Khamsin, S.A., Hossain, M.E., 2012. A novel approach to handle continuous wettability alteration during immiscible CO_2 flooding process. In: Abu Dhabi International Petroleum Conference and Exhibition. SPE https://doi.org/10.2118/160638-MS.

Andersen, P.Ø., Evje, S., Kleppe, H., Skjæveland, S.M., 2015. A model for wettability alteration in fractured reservoirs. SPE J. 20, 1261–1275. https://doi.org/10.2118/174555-PA.

Barenblatt, G., Patzek, T., Silin, D., 2003. The mathematical model of nonequilibrium effects in water-oil displacement. SPE J. 409–416. https://doi.org/10.2118/87329-PA.

Bartley, J.T., Ruth, D.W., 1999. Relative permeability analysis of tube bundle models. Transport Porous Media 36, 161–187. https://doi.org/10.1023/A:1006575231732.

Blunt, M.J., 1997. Pore level modeling of the effects of wettability. SPE J. 2, 494–510. https://doi.org/10.2118/38435-PA.

Blunt, M.J., 2001. Flow in porous media– pore-network models and multiphase flow. Curr. Opin. Colloid Interface Sci. 6, 197–207. https://doi.org/10.1016/S1359-0294(01)00084-X.

Blut, M.J., 2017. Multiphase Flow in Permeable Media: A Pore-Scale Perspective. Cambridge university press.

Bonn, D., Eggers, J., Indekeu, J., Meunier, J., Rolley, E., 2009. Wetting and spreading. Rev. Mod. Phys. 81, 739–805. https://doi.org/10.1103/RevModPhys.81.739.

Buckley, J.S., Liu, Y., Monsterleet, S., 1988. Mechanisms of wetting alteration by crude oils. SPE J. 3, 54–61. https://doi.org/10.2118/37230-PA.

Chalbaud, C., Robin, M., Lombard, J., Martin, F., Egermann, P., Bertin, H., 2009. Interfacial tension measurements and wettability evaluation for geological CO_2 storage. Adv. Water Resour. 32, 98–109. https://doi.org/10.1016/j.advwatres.2008.10.012.

Chiquet, P., Broseta, D., Thibeau, S., 2007a. Wettability alteration of caprock minerals by carbon dioxide. Geofluids 112–122. https://doi.org/10.1111/j.1468-8123.2007.00168.x.

Dahle, H.K., Celia, M.A., Hasanizadeh, S.M., 2005. Bundle-of-tubes model for calculating dynamic effects in the capillary-pressure saturation relationship. Transport Porous Media 58, 5–22. https://doi.org/10.1007/s11242-004-5466-4.

Davis, A., Morton III, S.A., Counce, R., DePaoli, D., Hu, M.-C., 2003. Ionic strength effects on hexadecane contact angles on a gold-coated glass surface in ionic surfactant solutions. Colloids Surf. A 221, 69–80. https://doi.org/10.1016/S0927-7757(03)00132-8.

Delshad, M., Najafabadi, N.F., Anderson, G.A., Pope, G.A., Sepehrnoori, K., 2009. Modeling wettability alteration by surfactants in naturally fractured reservoirs. SPE J. 12, 361–370. https://doi.org/10.2118/100081-PA.

Dickson, J.L., Gupta, G., Horozov, T.S., Binks, B.P., Johnston, K.P., 2006. Wetting phenomena at the CO_2/water/glass interface. Langmuir 22, 2161–2170. https://doi.org/10.1021/la0527238.

Du, Y., Xu, K., Mejia, L., Zhu, P., Balhoff, M.T., 2019. Microfluidic investigation of low-salinity effects during oil recovery: a no-clay and time-dependent mechanism. SPE J. 2841–2858. https://doi.org/10.2118/197056-PA.

Eral, H.B., 't Mannetje, D.J.C.M., Oh, J.M., 2013. Contact angle hysteresis: a review of fundamentals and applications. Colloid Polym. Sci. 291, 247–260. https://doi.org/10.1007/s00396-012-2796-6.

van Erp, T.S., Trinh, T., Kjelstrup, S., Glavatskiy, K.S., 2014. On the relation between the langmuir and thermodynamic flux equations. Front Phys. 1–14. https://doi.org/10.3389/fphy.2013.00036.

Haagh, M.E.J., Siretanu, I., Duits, M.H.G., Mugele, F., 2017. Salinity-dependent contact angle alteration in oil/brine/silicate systems: the critical role of divalent cations. Langmuir 33, 3349–3357. https://doi.org/10.1021/acs.langmuir.6b04470.

Hassanizadeh, S., Celia, M., Dahle, H., 2002. Dynamic effects in the capillary pressure–saturation relationship and its impacts on unsaturated flow. Vadose Zone J. 1, 38–57. https://doi.org/10.2113/1.1.38.

Helland, J.O., Skjæveland, S.M., 2006. Physically based capillary pressure correlation for mixed-wet reservoirs from a bundle-of-tubes model. In: Proceedings of the SPE/DOE Improved Oil Recovery Symposium. SPE, pp. 171–180. https://doi.org/10.2118/89428-PA.

Helland, J.O., Skjæveland, S.M., 2007. Relationship between capillary pressure, saturation, and interfacial area from a model of mixed-wet triangular tubes. Water Resour. Res. 43, 1–15. https://doi.org/10.1029/2006WR005698.

Iglauer, S., Mathew, M., Bresme, F., 2012. Molecular dynamics computations of brine-CO_2 interfacial tensions and brine-CO_2-quartz contact angles and their effects on structural and residual trapping mechanisms in carbon geosequestration. J. Colloid Interface Sci. 386, 405–414. https://doi.org/10.1016/j.jcis.2012.06.052.

Iglauer, S., Pentland, C.H., Busch, A., 2014. CO_2wettability of seal and reservoir rocks and the implications for carbon geo-sequestration. Water Resour. Res. 51, 729–774. https://doi.org/10.1002/2014WR015553.

Iglauer, S., Rahman, T., Sarmadivaleh, M., Al-Hinai, A., Fernø, M.A., Lebedev, M., 2016. Influence of wettability on residual gas trapping and enhanced oil recovery in three-phase flow: a pore-scale analysis by use of microcomputed tomography. SPE J. 21, 1916–1929. https://doi.org/10.2118/179727-PA.

Jadhunandan, P.P., Morrow, N.R., 1995. Effect of wettability on waterflood recovery for crude-oil/brine/rock systems. SPE Reservoir Eng. 10, 40–46. https://doi.org/10.2118/22597-PA.

Jafari, M., Jung, J., 2016. The change in contact angle at unsaturated CO_2-water conditions: implication on geological carbon dioxide sequestration. Geochem. Geophys. Geosyst. 17, 3969–3982. https://doi.org/10.1002/2016GC006510.

Jung, J.W., Wan, J., 2012. Supercritical CO_2 and ionic strength effects on wettability of silica surfaces: equilibrium contact angle measurements. Energy Fuels 26, 6053–6059. https://doi.org/10.1021/ef300913t.

Kim, Y., Wan, J., Kneafsey, T.J., Tokunaga, T.K., 2012. Dewetting of silica surfaces upon reactions with supercritical CO_2 and brine: pore-scale studies in micromodels. Environ. Sci. Technol. 46, 4228–4235. https://doi.org/10.1021/es204096w.

Krumpfer, J.W., McCarthy, T.J., 2010. Contact angle hysteresis: a different view and a trivial recipe for low hysteresis hydrophobic surfaces. Faraday Discuss. 146, 103–111. https://doi.org/10.1039/b925045j.

Lashgari, H.R., Xu, Y., Sepehrnoori, K., 2016. Modelling dynamic wettability alteration effect based on contact angle. SPE, pp. 1–17. https://doi.org/10.2118/179665-MS.

McKee, D., Swailes, S., 1991. On the derivation of the langmuir isotherm for adsorption kinetics. J. Phys. A Math. Gen. 24, 207–2010.

Morrow, N.R., Lim, H.T., Ward, J.S., 1986. Effect of crude-oil-induced wettability changes on oil recovery. SPE, pp. 89–103. https://doi.org/10.2118/13215-PA.

Morton III, S.A., Keffer, D.J., Counce, R.M., DePaoli, D.W., 2005. Behavior of oil droplets on an electrified solid metal surface immersed in ionic surfactant solutions. Langmuir 21, 1758–1765. https://doi.org/10.1021/la0480235.

Morton III, S.A., Keffer, D.J., Counce, R.M., DePaoli, D.W., C., H.M.Z., 2004. Thermodynamic method for prediction of surfactant-modified oil droplet contact angle. J. Colloid Interface Sci. 270, 229–241.

Plug, W.J., Bruining, J., 2007. Capillary pressure for the sand-CO_2-water system under various pressure conditions. application to CO_2 sequestration. Adv. Water Resour. 30, 2339–2353. https://doi.org/10.1016/j.advwatres.2007.05.010.

Saraji, S., Goual, L., Piri, M., Plancher, H., 2013. Wettability of scCO2/water/quartz systems: simultaneous measurement of contact angle and interfacial tension at reservoir conditions. Langmuir 1–39. https://doi.org/10.1021/la3050863.

Singh, R., Mohanty, K., 2016. Foams with wettability-altering capabilities for oil-wet carbonates: a synergistic approach. SPE J. 21, 1126–1139. https://doi.org/10.2118/175027-PA.

Skjæveland, S.M., Siqveland, L.M., Kjosavik, A., Thomas, W.L.H., Virnovsky, G.A., 2000. Capillary pressure correlation for mixed-wet reservoirs. SPE, pp. 60–67. https://doi.org/10.2118/60900-PA.

Tokunaga, T.K., Wan, J., 2013. Capillary pressure and mineral wettability influences on reservoir CO_2 capacity. Rev. Mineral. Geochem. 77, 481–503. https://doi.org/10.2138/rmg.2013.77.14.

Tokunaga, T.K., Wan, J., Jung, J., Kim, T.W., Kim, Y., Dong, W., 2013. Capillary pressure and saturation relations for supercritical CO_2 and brine in sand: high-pressure $p_c(s_w)$ controller/meter measurements and capillary scaling predictions. Water Resour. Res. 49, 4566–4579. https://doi.org/10.1002/wrcr.20316.

Wang, S., Tokunaga, T.K., 2015. Capillary pressure-saturation relations for supercritical CO_2 and brine in limestone/dolomite sands: implications for geologic carbon sequestration in carbonate reservoirs.. Environ. Sci. Technol. 49, 72087217. https://doi.org/10.1021/acs.est.5b00826.

Wang, S., Tokunaga, T.K., Wan, J., Dong, W., Kim, Y., 2016. Capillary pressure-saturation relations in quartz and carbonate sands: limitations for correlating capillary and wettability influences on air, oil, and supercritical CO_2 trapping. Water Resour. Res. 6671–6690. https://doi.org/10.1002/2016WR018816.

Washburn, E., 1921. The dynamics of capillary flow. Phys. Rev. 7, 273–283.

Xu, W.S., Luo, P.Y., Sun, L., Lin, N., 2016. A prediction model of the capillary pressure j–function. PLoS ONE 11, 1–9. https://doi.org/10.1371/journal.pone.0162123.

Yu, L., Kleppe, H., Kaarstad, T., Skjæ veland, S.M., 2008. Modelling of wettability alteration processes in carbonate oil reservoirs. Netw. Heterog. Media 3, 149–183. https://doi.org/10.3934/nhm.2008.3.149.